Portable X-ray fluorescence analysis of water: thin film and water thickness considerations

Julia Kagiliery[1], Somsubhra Chakraborty[2], Bin Li[3], Michael Hull[4], David C. Weindorf[5]*

1 Episcopal School of Jacksonville, Jacksonville, USA
2 Agricultural and Food Engineering Department, Indian Institute of Technology Kharagpur, Kharagpur, West Bengal, India
3 Department of Experimental Statistics, Louisiana State University, Baton Rouge, USA
4 Olympus Corporation of the Americas, Webster, USA
5 Department of Earth and Atmospheric Sciences, Central Michigan University, Mount Pleasant, USA

*Corresponding author E.mail: weind1dc@cmich.edu

Abstract

Water is requisite for life and essential for many industries. Increasingly, global water supplies include inorganic contaminants leading to millions of deaths annually. High analytical cost and a lack of field portable methods have stymied the evaluation of contaminated water. By comparison, portable X-ray fluorescence (PXRF) spectrometry has emerged as a method suitable for low cost, rapid analysis for many matrices yet few studies have evaluated liquids via PXRF. Herein, a novel means of assessing PXRF analytical performance for liquid matrices was evaluated on 1,440 samples comprised of three different standards (Cd, Cr, Pb) featuring three different film types (Kapton, Mylar, and Prolene) at five different liquid depths (4.29, 8.59, 17.18, 25.77 and 30.06 mm), and with four different concentrations (1,000, 500, 250, 125 μg/g). To adjust the PXRF values for a liquid matrix, regression models were fitted using PXRF reported values as the predictor and the true standard concentration values as the target. Results indicated that prior to statistical adjustment to PXRF reported values, increased liquid depth as well as Mylar or Kapton film provided optimal predictive accuracy. However, after PXRF adjustment (linear for Cr and Cd, quadratic for Pb), a depth of 4.29 mm and any of the three film types provided quality elemental predictions. After PXRF adjustment, the size of the mean of PXRF difference with the known standard concentration vs. the true standard concentration values became much smaller compared to the prior adjustment difference. Additionally, the size of the difference was usually smaller for the larger depth (25.77 and 30.06 mm).

Introduction

The World Health Organization (WHO) estimates 2.2 billion people do not have access to safe, potable water (World Health Organization, 2020). Deleterious water sources may include biological (e.g., diseases including cholera, diarrhea, typhoid, polio, hepatitis A) or inorganic (As, Cr, Pb)

contaminants contributing to millions of deaths worldwide annually (World Health Organization, 2019). Thus, access to clean water is essential for human health and prosperity. In addition to human and animal consumption, potable water is often used for sanitary purposes (e.g., flushing waste/ toilets, cleaning). Known as the universal solvent, water is also used in countless chemical/industrial processing activities (e.g., catalysis, hydrolysis, etc.). Indeed, leakage or improper disposal of aqueous industrial byproducts is a major cause of global water pollution (e.g., Florea et al., 2005; Awomeso et al., 2010).

Today, many developing countries suffer from polluted/contaminated water supplies (Zimmerman et al., 2021). Even in developed countries like the United States, highly polluted "superfund sites" are rife with subsurface pollution which commonly moves into groundwater sources (United States Environmental Protection Agency, 2020a). The Gold King Mine spill (United States Environmental Protection Agency, 2020b; Duval et al., 2020) and Flint water crisis (United States Environmental Protection Agency, 2020c; Masten et al., 2016) are recent examples of aqueous discharge of toxic elements into water supplies used for human/ animal consumption and/or agricultural irrigation. The National Resource Defense Council (2018), noted that the Flint water crisis was largely a result of cost saving measures, leaving corrosive water from the Flint River to leach Pb from aging pipes. Such crises underscore the need for rapid, portable analytical instrumentation capable of providing real time data for environmental analysis.

The insidious nature of many chronic pollutants suspended or chemically dissolved in water is that they defy taste, smell, or visual detection. To date, several well-established laboratory techniques are used to quantify elemental concentrations in liquid matrices, among them, flame photometry (Banerjee and Prasad, 2020), atomic absorption (AA) spectroscopy (Isaac and Kerber, 1971), and inductively coupled plasma (ICP) mass spectroscopy (MS) (United States Geological Survey, 1993). Field portable approaches include various ion-sensing electrodes (Bagheri et al., 2013)

and colorimetric test strips (Chen et al., 2019). Though accurate, laboratory-based approaches are time consuming, expensive, and non-field portable. Contrariwise, ion-sensing electrodes and colorimetric test strips are field portable but may offer restricted detection limits or single elemental detection. The elegant solution to these limitations concerns the use of portable X-ray fluorescence (PXRF) spectrometry, which has the potential to overcome the limitations aforementioned whilst offering robust, multi-elemental analyses in a field portable sensor.

PXRF spectrometry has rapidly grown in popularity for characterization of soil (Silva et al., 2020; Weindorf et al., 2014), mine tailings (Koch et al., 2017), and hard-rock geology (Steiner et al., 2017). Further, the technique has more recently been extended to lower density matrices such as vegetation (Zhou et al., 2020a; McGladdery et al., 2018), lignite (Kagiliery et al., 2019), and pharmaceuticals (powders and medical leeches) (Shutic et al., 2017; Zhou et al., 2020b). Finally, recent studies extended the use of PXRF to determine the salinity of brackish waters (Pearson et al., 2017) and metal laden water (Pearson et al., 2018; Zhou et al., 2018). Pearson et al. (2018) revealed near perfect r^2 (0.99-1.00) between ICP and PXRF results for Ca, K, Fe, Cu, Pb, Zn, and Mn. Further extension of Pearson et al. (2018) led to US Patent US10697953B2 "Portable apparatus for liquid chemical characterization" (Weindorf et al., 2018).

While highly effective, these approaches were based upon an instrument configuration known as Geochem Mode which uses a fundamental parameters approach for interpreting the raw fluorescent signal and transforming it into appropriate elemental data (van Sprang, 2000; Rousseau, 2009; Thomson, 2007). Contemporary PXRF units use low power (10-50 keV) X-ray tubes to produce excitation. The penetration depth for the X-rays is a function of the energy of the incident X-rays from the instrument but also a function of the sample density and composition. The escape depth - the depth from which fluorescent energy can escape the sample and reach

the detector - is what is analytically significant more than the penetration depth (the total depth to which primary X-rays penetrate). The escape depth is contingent up the characteristic X-ray emission energy of the elements in the sample. The escape depth will always be less than the penetration depth. The escape depth varies from element to element. Elements with higher energy characteristic emission X-rays will have greater escape depth than lighter elements with weaker (lower intensity) characteristic emission X-rays. In order to achieve an accurate and representative analysis of the sample it is important that the sample thickness be greater than the maximum escape depth for any element in the sample. This maximum escape depth is referred to as critical thickness or infinite thickness. Beyond infinite thickness, no additional thickness in sample will result in more X-ray emission from the matrix. For soil (bulk density ~1.33 g cm^{-3}), Kalnicky and Singhvi (2001) report "the maximum depth of X-ray penetration using sealed radioisotope sources is approximately 2mm." Evaluating an archeological pedestal and stupa, Uda et al. (2005) noted that penetration depth of X-rays with energies of 20–40 keV is in the range of several tens of micrometers for typical elements. By contrast, recent research on PXRF analysis of vegetative matrices has indicated variable escape depth which is element-dependent; Rincheval et al. (2019) noted that most fluorescent signal derives from the first 2 to 6 mm of vegetative matrices given their low densities. Such findings assert film composition as a substantial factor in the analysis of low-density matrices, especially when said matrices possess high levels of moisture and the elements of interest are light elements (e.g., K, Ca) (Zhou et al., 2020a). Common thin films sold for PXRF analysis include Prolene, Mylar, Kapton, Polypropylene, Etnom, and Zythene (Chemplex Industries, Palm City, FL, USA). These films vary in thickness, density, and composition. Hall et al. (2013) note that less dense films provide less attenuation of fluorescence.

While the findings of Pearson et al. (2017 and 2018) are promising for liquid characterization by PXRF, minimal and optimal thickness for accurate quantification of various elements in solution remains unknown, especially at variable concentrations. Measuring Cu and Pb in water with PXRF, Zhou et al. (2018) found the penetration depth of X-rays in water to be between 2 and 4 mm, suggesting 4 mm for optimal results.

Given the rapidly expanding use of PXRF for an array of environmental quality assessment parameters and its robust performance in early applications to aqueous samples, a more robust understanding of critical penetration depth and thin film influences on elemental results is warranted. Pearson et al. (2018) note that as the approach gains more popularity and study, contemporary PXRF units could be custom configured with a low-density Water Mode to rapidly assess suspect liquid samples on-site in seconds. Even if the ultimate in quantitative accuracy demand traditional analysis via ICP-MS, PXRF has the potential to be used as a rapid screening tool to refine laboratory analyses to remarkable samples whilst doing so at minimal cost and analyst time. As such, the objectives of this study were to: a) determine the minimum and optimum thickness for quantification of variable elements in solution at different concentrations, and b) identify which thin film produces the least amount of X-ray attenuation for characterization of solutions. We hypothesized that a logarithmic function would best describe the quantification of elements with increasing water thickness, performance would be similar amongst multiple elements evaluated, and that variable thin film composition would differentially impact fluorescent attenuation.

Materials and Methods

General Experimental Considerations

The samples evaluated in this study were three ICP elements standards of Pb, Cr, and Cd (Ricca Chemical Company, Batesville, IN, USA). Lead, chromium, and cadmium were selected as representative elements of interest due to: 1) their association with environmental contamination (e.g., RCRA metals), and 2) their varied characteristic X-ray emission energies (Cr Kα 5.41 KeV; Cd Kα 26.1 KeV; Pb Lβ 12.61

KeV). A fourth ICP standard of Mg at 1,000 µg/g was evaluated, but found to fall below the limit of detection even with extended sampling time (150 sec beam[-1]); thus, it was eliminated from the study. A Vanta M (Olympus, Waltham, MA, USA) PXRF spectrometer was used to conduct the scanning whilst using a Field Stand-V to mount samples. The spectrometer was operated in Geochem mode at 20 sec beam[-1] for a total of 40 sec per scan on line power (115 VAC). While custom configurations are possible, Olympus does not currently widely deploy Aqueous mode as a common matrix calibration; hence, Geochem mode was used in the present study. The primary difference between the modes concerns background subtraction. Geochem mode assumes the background looks like quartz/silica; whereas Aqueous mode assumes the background is predominantly water. Scanning a liquid sample with Geochem mode may yield more false positives than Aqueous mode, yet the two modes offer similar overall performance. For this study, three common thin film types were used: Kapton, Prolene, and Mylar. Thicknesses of the films were 7.5 µm, 4.0 µm, and 6.0 µm, respectively. These film materials were selected due to their ease of commercial accessibility and wide chemical compatibility.

Double open-ended samples cups (38.5 mm diameter; 32 mm height; Chemplex, Palm City, FL, USA) were prepared with the three different films. Each ICP standard was scanned at variable solution concentrations (1,000 µg/g as received, then 500, 250 and 125 µg/g solutions prepared via serial dilution with distilled water) (Fig. 1).

Eight scans were taken of each dilution on each film type at five different depths. For simplicity sake, let water thickness reflect the column of water in sample cups above the thin film. However, rather than measuring height of the water column directly, volumes pipetted into the sample cup (5, 10, 20, 30, 35 ml) were used for actual measurement, with heights calculated accordingly from the cup diameter. Thus, heights of the water column scanned were 4.29, 8.59, 17.18, 25.77 and 30.06 mm, respectively. Nonetheless, hereafter the volumes will be reported for simplicity sake.

Figure 1. *Experimental configuration using a Field Stand-V to mount samples. Pictured here are liquid samples containing Cd, placed directly over the portable X-ray fluorescence (PXRF) spectrometer aperture, and scanned in sample cups featuring Kapton thin film.*

In sum, n=1,440 inclusive of three elemental standards scanned at four different concentrations on three different types of thin film at five different sample depths with eight replicate scans of each condition.

Statistical Analyses
Initially, the t-test and Wilcoxon signed rank test were executed on each film-standard-dilution-volume combination using PXRF reported elemental values. Notably, the signed rank test is a nonparametric test with low power but having relaxed assumption for the data, such as normality and homogeneity of variances. For each standard-film-volume combination, there were 4*8=32 data points (4 µg/g levels * 8 replications). Subsequently, regression models were fitted considering the PXRF reported values as the predictor and the true standard concentration values as the target for adjusting the PXRF values for liquid matrix. After PXRF adjustment, both t-test and Wilcoxon sign-rank test were executed. All statistical analyses were executed in R version 3.6.2. (R Core Team, 2020).

Results and Discussion

Figure 2 indicates the mean for each standard-film-volume-dilution combination. Without PXRF adjustment, all three films had some systematic bias in most of the combinations, and the difference among the three films was much smaller than the bias. For Cd, most of the measurements were lower than the true standard concentrations, especially for higher concentrations. For Cr, all three films underestimated the standard concentrations for low concentration level (125 and 250 µg/g), but overestimated for high levels (500 and 1000 µg/g). Also, the standard error of mean for most Cr-film-volume combinations was higher for high levels (1000 µg/g). This general pattern is in keeping with what is to be expected based on the structure of the manufacture's calibration. Multiple

pXRF manufacturers offer a "geochemical" or "mining" fundamental parameters calibration. This calibration approach models the matrix attenuation off of a quartz/silica background. Quartz/silica (SiO_2) has a greater density and mass attenuation of X-rays than water (H_2O). Overlayed on this matrix effect is attenuation from the cup films.

Thicker films provide greater X-ray attenuation than thinner films. Film composition also impacts the magnitude of the attenuation (e.g., Prolene versus Mylar versus Kapton). The attenuation from the film is most pronounced for lighter elements/weaker X-rays, namely Cr (5.41 KeV Kα) in this study. For Pb, all three films overestimated the standard concentrations, but the bias was the smallest in all standards. This pattern for Pb is in keeping with what is expected from the above issues of matrix and film attenuation.
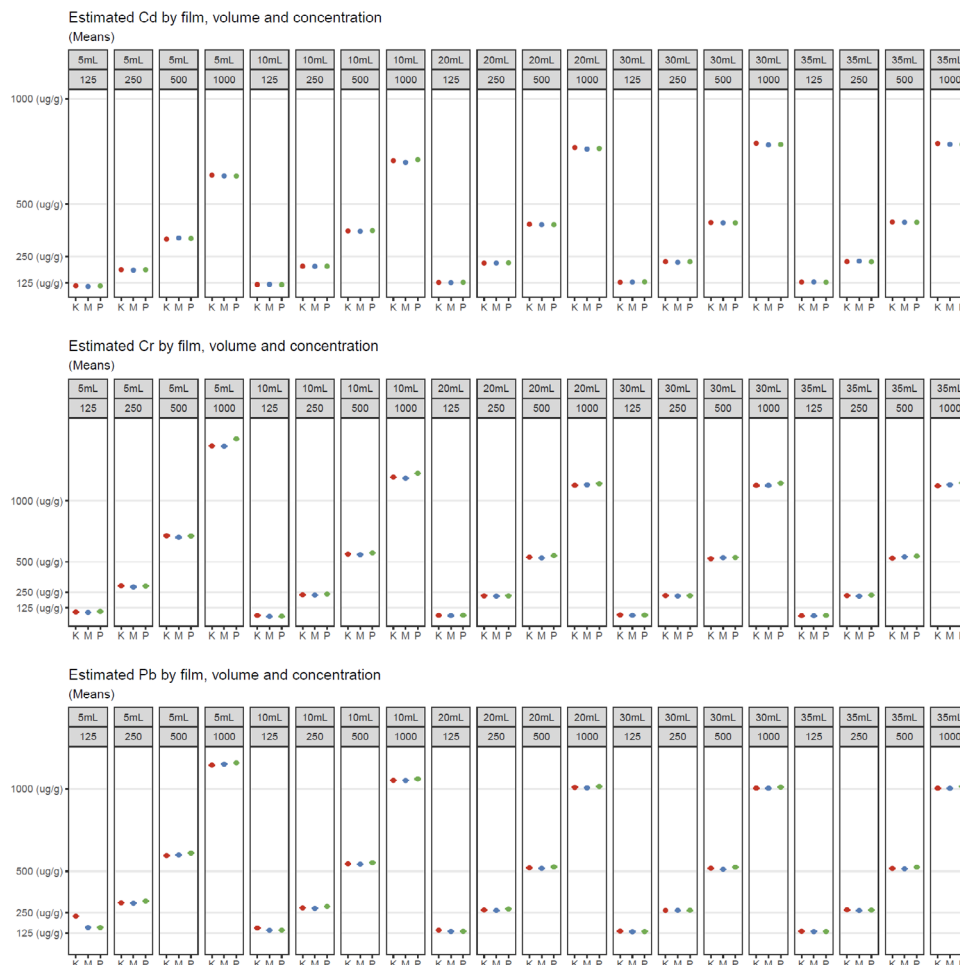
Figure 2. *Plots indicating the mean for each standard-film-volume-dilution combination. The red, blue, and green dots indicated Kapton, Mylar, and Prolene thin films, respectively.*

Aqueous samples will have less attenuation than geochemical samples (quartz/silica-rich) causing manufacturer's calibration to overreport. At the same time the higher energy characteristic emission X-rays from Pb (12.61 KeV Kα) are less impacted from the film attenuation relative to the weaker Cr emission X-rays. In general, larger volumes produced more accurate estimates. Nevertheless, the volume effect was not obvious in Cd. For Cr and Pb, using 20 ml volume achieved very similar performance as 35 ml.

Initially, both t-test and Wilcoxon signed rank test were executed on each standard-film-volume-dilution combination to examine the relationship between PXRF reported elemental concentrations and actual standard concentrations. Table 1 exhibits the p-values for both tests which indicate that in almost all cases, PXRF-reported values had a significant difference with the known standard concentration.

This variation can be attributed to the Geochem mode calibration of PXRF which is not targeted to a water matrix. Notably, the instrument can be custom configured to account for a liquid matrix, but Geochem mode was tested in this study as it is a standard mode offered on most instruments directly from the manufacturer (e.g., requiring little if any customization by the end user prior to use). However, from the plots exhibiting the relation between the mean PXRF reported values and the true standard concentration values (Fig. 3) and the mean of PXRF difference with the known standard concentration vs. the true standard concentration values (Fig. 4), strong associations were observed.

In particular, Cr and Cd exhibited linear association while Pb showed a quadratic association. Consequently, PXRF results were adjusted to improve the elemental estimation in liquid. For Cr and Cd, linear regression models were used while for Pb, quadratic models were fitted. Notably, linear regression was applied instead of complex models to preclude overfitting of the data.

Table 2 exhibits the fitted regression coefficients for all the models. Figure 5 exhibits the relationship between the mean of adjusted PXRF values and true standard concentration values.

Moreover, the mean of PXRF difference with the known standard concentration after adjustment vs. the true standard concentration values was also plotted (Fig. 6).

It was observed that after PXRF adjustment, the size of the difference became much smaller compared to the prior adjustment difference. Also, the size of the difference was usually smaller for the large volume (30 or 35 ml).

Subsequently, both the t-test and Wilcoxon signed rank test using the model fitted value were re-executed. After PXRF adjustment, the majority of the tests became non-significant (Table 3) indicating the benefit of PXRF tuning for elemental estimation in a liquid matrix.

Among the three films, before adjustment, Kapton and Mylar performed slightly better than Prolene (Table 1). However, after adjustment, all three film types had very close results (Table 3), which confirmed the importance of adjustment. The post-adjustment p-values of Wilcoxon signed rank tests for 5 ml indicated that 5 ml volume produced the optimum results, which is closely related to infinite thickness. Recall that in the present study, 5 ml volume equates to 4.29 mm of water thickness over the film, supporting Rincheval et al. (2019) who found 2 to 6 mm of penetration depth in low density vegetal matrices produced optimal results and Zhou et al. (2018) who suggested optimal depth of X-rays in water to be ~4 mm. Also, it was evident that the use of Prolene for Cd and Cr and Mylar for Pb were beneficial since they produced non-significant results for 5 ml volume.

Although the difference between the true standard concentration and PXRF reported concentration for Cd and Cr showed an up-side-down U shape (Fig. 6) indicating a quadratic pattern, due to the small sample size, few dilution levels, and non-significant test results, a linear model adjustment was done for both Cd and Cr. Nevertheless, the difference in Pb was random without any systematic pattern.

Table 1. *One-sample Wilcoxon Signed Rank test and one -sample t-test p-values (two-sided) for all standard-film-volume-dilution combinations before portable X-ray fluorescence (PXRF) adjustment. All elemental values (125, 250, 500, 1000) are in µg/g.*

| Film	Vol	Cd (125)	Cd (250)	Cd (500)	Cd (1000)	Cr (125)	Cr (250)	Cr (500)	Cr (1000)	Pb (125)	Pb (250)	Pb (500)	Pb (1000)
						One-sample Wilcoxon Signed Rank test							
Kapton	5	0.014	0.014	0.014	0.014	0.014	0.014	0.014	0.014	0.014	0.014	0.012	0.014
Mylar	5	0.014	0.014	0.014	0.014	0.014	0.014	0.014	0.014	0.014	0.014	0.014	0.014
Prolene	5	0.014	0.014	0.014	0.014	0.014	0.014	0.014	0.014	0.014	0.014	0.014	0.014
Kapton	10	0.014	0.014	0.014	0.014	0.014	0.014	0.014	0.014	0.013	0.014	0.014	0.014
Mylar	10	0.014	0.014	0.014	0.014	0.014	0.014	0.014	0.014	0.014	0.014	0.014	0.014
Prolene	10	0.014	0.014	0.014	0.014	0.014	0.042	0.014	0.014	0.014	0.014	0.014	0.014
Kapton	20	0.122†	0.014	0.014	0.014	0.014	0.014	0.014	0.014	0.014	0.014	0.014	0.014
Mylar	20	0.033	0.013	0.014	0.014	0.014	0.014	0.014	0.014	0.013	0.014	0.014	0.014
Prolene	20	0.022	0.014	0.014	0.014	0.014	0.014	0.014	0.014	0.014	0.014	0.014	0.014
Kapton	30	0.057†	0.014	0.014	0.014	0.014	0.014	0.014	0.014	0.013	0.181†	0.014	0.020
Mylar	30	0.025	0.014	0.014	0.014	0.014	0.014	0.014	0.014	0.014	0.014	0.014	0.034
Prolene	30	0.014	0.014	0.014	0.014	0.014	0.021	0.014	0.014	0.014	0.014	0.014	0.014
Kapton	35	0.014	0.014	0.014	0.014	0.014	0.014	0.014	0.014	0.014	0.014	0.014	0.029
Mylar	35	0.014	0.014	0.014	0.014	0.014	0.014	0.014	0.014	0.014	0.013	0.014	0.036
Prolene	35	0.014	0.014	0.014	0.014	0.014	0.014	0.014	0.014	0.014	0.014	0.013	0.014
						One-sample t-Test							
Kapton	5	0.000	0.000	0.000	0.000	0.000	0.000	0.000	0.000	0.001	0.000	0.000	0.000
Mylar	5	0.000	0.000	0.000	0.000	0.000	0.000	0.000	0.000	0.000	0.000	0.000	0.000
Prolene	5	0.000	0.000	0.000	0.000	0.000	0.000	0.000	0.000	0.000	0.000	0.000	0.000
Kapton	10	0.000	0.000	0.000	0.000	0.000	0.000	0.000	0.000	0.000	0.000	0.000	0.000
Mylar	10	0.000	0.000	0.000	0.000	0.000	0.000	0.000	0.000	0.000	0.000	0.000	0.000
Prolene	10	0.000	0.000	0.000	0.000	0.000	0.000	0.000	0.000	0.000	0.000	0.000	0.000
Kapton	20	0.091†	0.000	0.000	0.000	0.000	0.000	0.000	0.000	0.000	0.000	0.000	0.001
Mylar	20	0.018	0.000	0.000	0.000	0.000	0.000	0.000	0.000	0.000	0.000	0.000	0.004
Prolene	20	0.003	0.000	0.000	0.000	0.000	0.000	0.000	0.000	0.000	0.000	0.000	0.000
Kapton	30	0.035	0.000	0.000	0.000	0.000	0.000	0.001	0.000	0.000	0.030	0.000	0.007
Mylar	30	0.008	0.000	0.000	0.000	0.000	0.000	0.000	0.000	0.000	0.000	0.000	0.011
Prolene	30	0.000	0.000	0.000	0.000	0.000	0.000	0.000	0.000	0.000	0.000	0.000	0.000
Kapton	35	0.003	0.000	0.000	0.000	0.000	0.000	0.000	0.000	0.000	0.000	0.000	0.011
Mylar	35	0.009	0.000	0.000	0.000	0.000	0.000	0.000	0.000	0.000	0.000	0.000	0.060†
Prolene	35	0.003	0.000	0.000	0.000	0.000	0.000	0.000	0.000	0.000	0.000	0.000	0.000

†non-significant value (α=0.05).
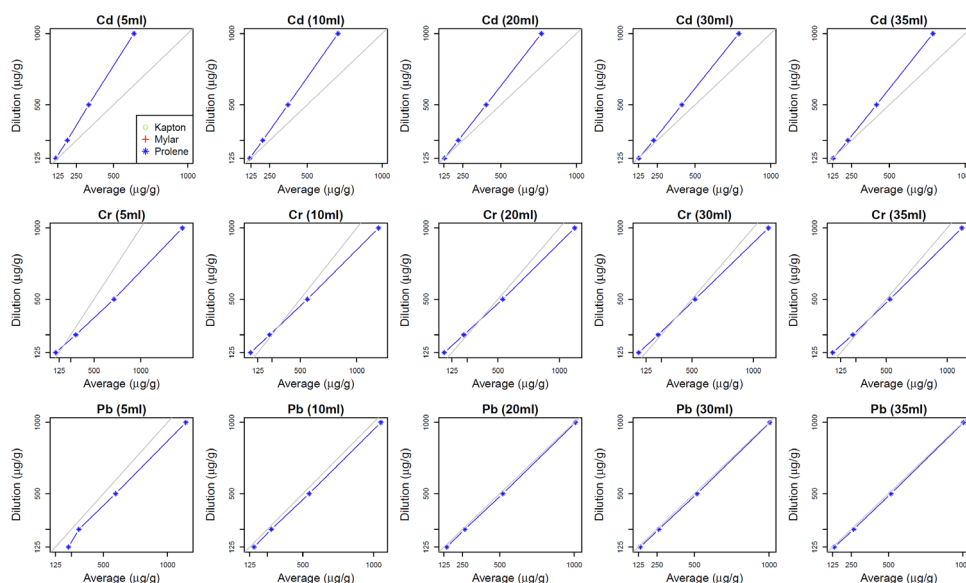
Figure 3. *Plots showing relationship between the mean portable X-ray fluorescence (PXRF) reported values and the true elemental concentration values of standards before PXRF adjustment. The gray line is 1:1 line to show the bias of the estimate.*
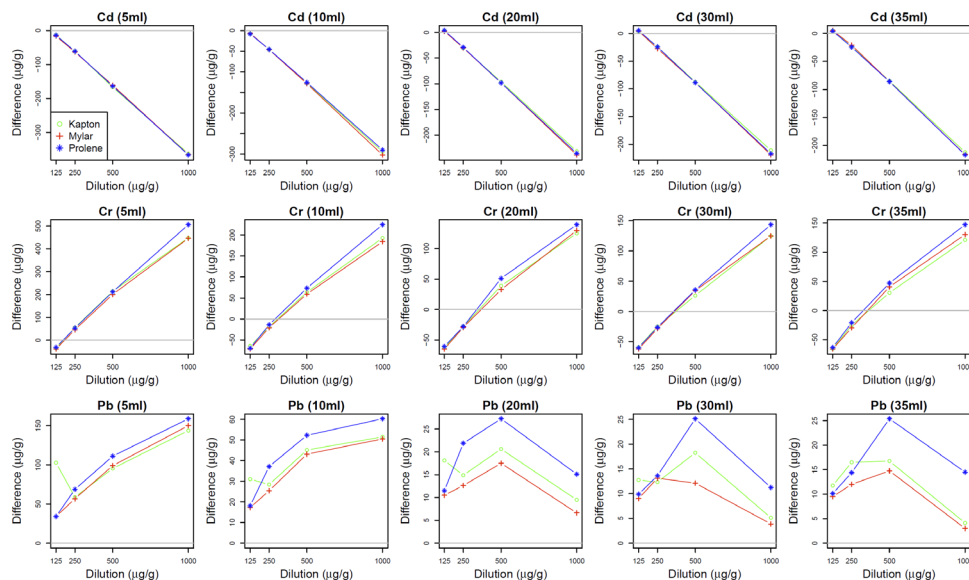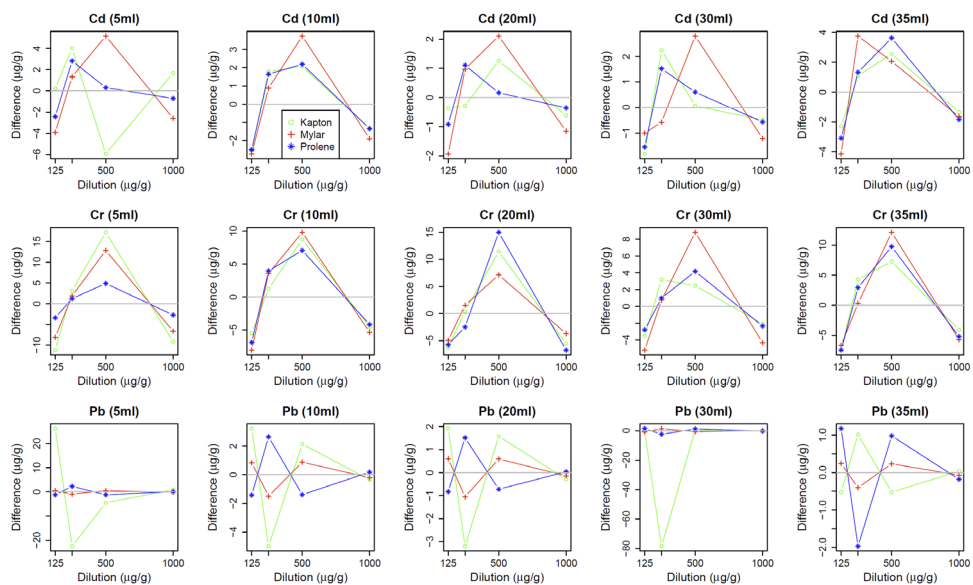

Figure 4. *Plots showing relationship between (true elemental standard concentration - portable X-ray fluorescence [PXRF] reported concentration) vs. true elemental concentration values before PXRF adjustment.*

Table 2. *Fitted regression coefficients for adjustment of portable X-ray fluorescence (PXRF) readings where b_1 and b_2 indicate slopes and b_o indicates y-intercept.*

Vol	Film	Cd (b_o)	Cd (b_1)	Cr (b_o)	Cr (b_1)	Pb (b_o)	Pb (b_1)	Pb (b_2)
5	Kapton	-61.05	1.66	56.46	0.64	-64.21	0.94	1.61×10^{-5}
10	Kapton	-52.23	1.48	72.41	0.77	-19.64	0.94	2.41×10^{-5}
20	Kapton	-49.94	1.36	67.29	0.82	-12.86	0.97	3.05×10^{-5}
30	Kapton	-47.66	1.32	66.81	0.82	-6.77	0.95	4.61×10^{-5}
35	Kapton	-49.76	1.33	68.18	0.82	-7.20	0.95	4.63×10^{-5}
5	Mylar	-59.81	1.66	61.58	0.64	-4.83	0.81	5.42×10^{-5}
10	Mylar	-56.73	1.51	75.52	0.77	-3.18	0.89	5.26×10^{-5}
20	Mylar	-52.46	1.38	70.68	0.81	-4.26	0.95	4.48×10^{-5}
30	Mylar	-49.95	1.34	67.93	0.82	-6.55	0.97	3.04×10^{-5}
35	Mylar	-53.62	1.34	69.94	0.81	-4.42	0.95	4.29×10^{-5}
5	Prolene	-63.88	1.67	63.64	0.61	0.23	0.76	8.58×10^{-5}
10	Prolene	-49.81	1.47	76.65	0.75	-1.52	0.86	7.70×10^{-5}
20	Prolene	-52.85	1.37	66.91	0.81	-1.41	0.90	7.56×10^{-5}
30	Prolene	-51.77	1.34	69.33	0.81	2.22	0.91	7.46×10^{-5}
35	Prolene	-50.69	1.33	67.63	0.80	1.19	0.91	6.75×10^{-5}
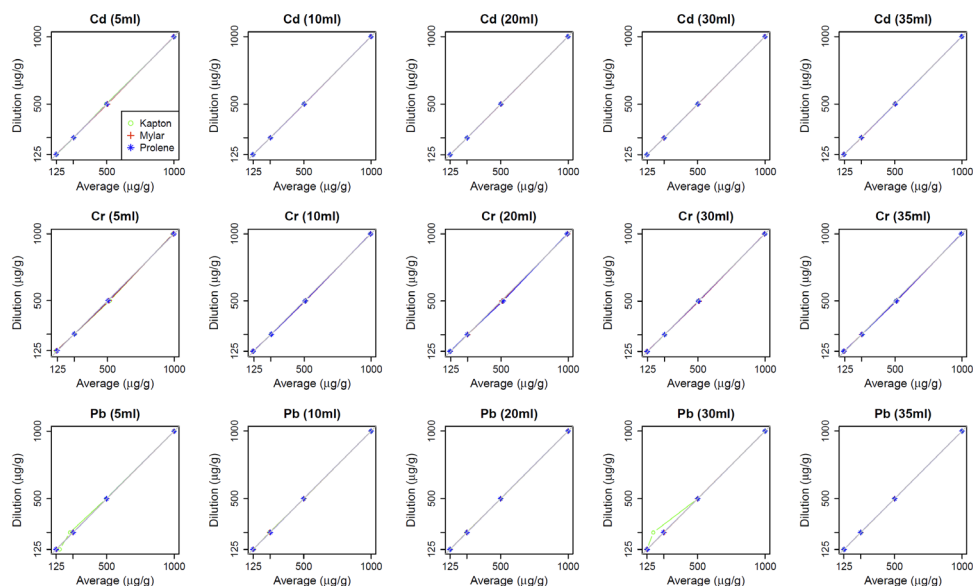
Figure 5. *Plots showing relationship between the mean portable X-ray fluorescence (PXRF) reported values and the true elemental concentration values of standards after PXRF adjustment. The gray line is 1:1 line to show the bias of the estimate.*

Figure 6. *Plots showing relationship between (true elemental standard concentration - portable X-ray fluorescence [PXRF] reported concentration) vs. true elemental concentration values after PXRF adjustment.*

Table 3. *One-sample Wilcoxon Signed Rank test and one -sample t-test p-values (two-sided) for all standard-film-volume-dilution combinations after portable X-ray fluorescence (PXRF) adjustment using α=0.05. Ka, My, and Pr indicate Kapton, Mylar, and Prolene film, respectively.*

Concentration (µg/g)	Vol	Cd-Ka	Cd-My	Cd-Pr	Cr-Ka	Cr-My	Cr-Pr	Pb-Ka	Pb-My	Pb-Pr
					One-sample Wilcoxon Signed Rank test					
125	5	0.726†	0.042	0.291†	0.014	0.021	0.080†	0.106†	0.291†	0.182†
250	5	0.233†	0.440†	0.725†	0.441†	0.233†	0.726†	0.014	0.439†	0.014
500	5	0.020	0.057†	0.944†	0.014	0.014	0.441†	0.012	0.441†	0.293†
1000	5	0.529†	0.141†	0.726†	0.294†	0.363†	0.529†	0.726†	0.834†	0.834†
125	10	0.107†	0.233†	0.057†	0.080†	0.042	0.014	0.103†	0.181†	0.106†
250	10	0.440†	0.833†	0.726†	0.528†	0.362†	0.292†	0.014	0.041	0.014
500	10	0.363†	0.079†	0.362†	0.014	0.080†	0.014	0.058†	0.292†	0.360†
1000	10	0.528†	0.528†	0.528†	0.363†	0.107†	0.363†	0.944†	1.000†	0.944†
125	20	0.833†	0.057†	0.362†	0.014	0.080†	0.042	0.234†	0.177†	0.528†
250	20	0.528†	0.618†	0.292†	0.726†	0.183†	0.441†	0.014	0.181†	0.182†
500	20	0.526†	0.292†	0.944†	0.030	0.080†	0.014	0.141†	0.362†	0.438†
1000	20	0.362†	0.726†	0.528†	0.183†	0.441†	0.141†	1.000†	0.833†	0.726†
125	30	0.623†	0.726†	0.141†	0.362†	0.014	0.141†	0.789†	0.526†	0.106†
250	30	0.181†	0.833†	0.233†	0.294†	0.833†	1.000†	0.014	0.058†	0.106†
500	30	0.833†	0.106†	0.726†	0.624†	0.042	0.183†	0.725†	0.726†	0.233†
1000	30	0.833†	0.725†	0.944†	0.834†	0.441†	0.624†	0.526†	0.944†	0.944†
125	35	0.230†	0.141†	0.041†	0.030	0.021	0.014	0.291†	0.725†	0.140†
250	35	0.833†	0.106†	0.292†	0.234†	0.726†	0.360†	0.528†	1.000†	0.181†
500	35	0.182†	0.106†	0.233†	0.030	0.042	0.014	0.726†	0.944†	0.723†
1000	35	0.293†	0.726†	0.079†	0.183†	0.042	0.441†	0.833†	0.528†	0.441†
					One-sample t-Test					
125	5	0.923†	0.011	0.246†	0.001	0.005	0.078†	0.210†	0.410†	0.310†
250	5	0.210†	0.583†	0.305†	0.313†	0.289†	0.761†	0.000	0.284†	0.004
500	5	0.024	0.047	0.796†	0.006	0.017	0.299†	0.001	0.605†	0.324†
1000	5	0.602†	0.188†	0.812†	0.281†	0.349†	0.479†	0.581†	0.939†	0.944†
125	10	0.214†	0.109†	0.035	0.067†	0.015	0.013	0.330†	0.203†	0.149†
250	10	0.294†	0.585†	0.577†	0.743†	0.301†	0.285†	0.000	0.010	0.001
500	10	0.499†	0.081†	0.337†	0.030	0.050†	0.013	0.074†	0.286†	0.170†
1000	10	0.650†	0.553†	0.570†	0.405†	0.217†	0.479†	0.808†	0.923†	0.898†

		One-sample t-Test								
125	20	0.859†	0.084†	0.434†	0.003	0.060†	0.017	0.240†	0.370†	0.440†
250	20	0.855†	0.451†	0.346†	0.831†	0.594†	0.365†	0.001	0.194†	0.152†
500	20	0.480†	0.220†	0.954†	0.013	0.084†	0.004	0.119†	0.494†	0.255†
1000	20	0.778†	0.680†	0.888†	0.330†	0.379†	0.153†	0.869†	0.935†	0.986†
125	30	0.373†	0.561†	0.108†	0.351†	0.010	0.810†	0.168†	0.403†	0.103†
250	30	0.201†	0.758†	0.322†	0.273†	0.720†	0.844†	0.009	0.059†	0.184†
500	30	0.974†	0.085†	0.738†	0.584†	0.019	0.142†	0.460†	0.536†	0.238†
1000	30	0.859†	0.489†	0.810†	0.714	0.410†	0.570†	0.929†	0.953†	0.869†
125	35	0.133†	0.062†	0.031	0.005	0.008	0.000	0.271†	0.777†	0.124†
250	35	0.471†	0.130†	0.191†	0.225†	0.898†	0.304†	0.442†	0.549†	0.190†
500	35	0.208†	0.135†	0.209†	0.012	0.018	0.028	0.713†	0.730†	0.319†
1000	35	0.426†	0.686†	0.077†	0.185†	0.025	0.376†	0.978†	0.961†	0.878†

† non-significant value (α=0.05).

In previous studies evaluating the influence of water thickness on PXRF results, a metallic target and the aperture of the PXRF were placed in a wide mouth beaker of water (Zhou et al., 2018). Notably, they studied low level concentrations of Cu and Pb (100 µg/g) but did so by dissolving metallic salts in deionized (DI) water. The approach herein was different, because the concentration of the target element in solution was known, with guaranteed analysis provided by the manufacturer. Thus in conducting the research, a wider range of solution concentrations was tested, along with influences from various types of commercially available thin films. Similar to the findings of Pearson et al. (2018), the present study gives compelling evidence (on a much larger sample set) that PXRF can provide accurate analysis of Cr, Pb, and Cd at ranges from 125 to 1,000 µg/g, yet even at very small volumes (e.g., water thickness).

The implications of the findings conducted herein are large. There are many industrial, medical, and chemical applications where the ability to test small volumes of sample is critical. For example, consider the possibility of using PXRF for rapid analysis of blood Fe content, or for uranalysis for quantification of K as a workup for hypokalemia or Ca for hypercalciuria. Modification of PXRF for industrial scanning may allow for continuous flow analysis of liquid products. PXRF may hold potential for use in determining the elemental/ nutritional value of various juices or milk (e.g., elemental concentrations of macro/micro- nutrients in breastmilk) (Pinto and Almeida, 2018). For example, Szymczycha-Madeja and Welna (2013), used ICP-atomic emission spectroscopy for multi- elemental characterization of fruit juices, yet PXRF may be able to provide similar analyses much more quickly, inexpensively, and as a field-portable instrument. In fairness, the limits of detection offered by PXRF do not approach the low level regulatory limits (commonly < 1 µg/g) (Kinuthia et al., 2020) imposed by many governments when evaluating drinking or waste waters. Yet, deployment of PXRF would be an elegant solution for rapid analysis when accidental spills occur, where special applications for higher elemental concentrations in liquid matrices are common, or in developing countries where traditional laboratory instrumentation used to test water samples remains inaccessible. Additionally, mixed matrices featuring suspended sediment pose challenges for traditional laboratory analyses such as ICP or AA, requiring filtration or centrifugation in advance of analysis;

PXRF overcomes this limitation allowing for direct scanning of the suspension. Future work should be done to assess the effectiveness of PXRF for low level (<100 µg/g) metal quantification in solution, especially in a multi-element and/or mixed matrix environment. Nonetheless, the approach demonstrated herein shows strong potential for addressing acute spills (e.g., Gold King Mine Spill) where rapid analysis of metal laden water is a priority. The possibilities are vast, and strongly support the development of a calibrated Aqueous mode not only from Olympus, but other PXRF manufacturers as well.

Conclusions

This study evaluated the influence of water thickness and thin film type in determining the elemental abundance of Cr, Cd, and Pb at four different concentrations in solution (1000, 500, 250, 125 µg/g). Before PXRF adjustment (linear for Cr and Cd, quadratic for Pb), there were significant differences between ICP standard and PXRF reported concentrations. As excepted, increased water thickness (e.g., more volume) improved PXRF predictive accuracy. Of the three thin films evaluated, Kapton and Mylar film offered slightly better accuracy. However, after statistical adjustment, 4.29 mm of water depth and any of the three films evaluated offered quality results in which there was no significant difference between water depths and film types concerning PXRF predicted concentration. Ultimately, this study underscores the importance of statistical adjustment of raw data reported by PXRF when scanning liquid matrices for optimal predictive performance. Yet in doing so, only minimal water thickness is required for quality elemental analysis. Furthermore, as PXRF analysis of liquids is non-consumptive as opposed to techniques such as ICP-MS or AA, the rapid examination of liquids via this technique has the potential to span many fields, including environmental science, medicine, and industry.

Acknowledgements

References

AWOMESO J.A., TAIWO A.M., GBADEBO A.M., ADENOWO J.A. (2010) Studies on the pollution of waterbody by textile industry effluents in Lagos, Nigeria. Journal of Applied Sciences in Environmental Sanitation, 5(4):353-359. ISSN 0126-2807.

BAGHERI H., AFKHAMI A., KHOSHSAFAR H., REZAEI M., SHIRZADMEHR A. (2013) Simultaneous electrochemical determination of heavy metals using a triphenylphospine/MWCNTs composite carbon ionic liquid electrode. Sensors and Actuators B, 186:451-460. https://doi.org/10.1016/j.snb.2013.06.051

BANERJEE P., PRASAD B. (2020) Determination of concentration of total sodium and potassium in surface and ground water using a flame photometer. Applied Water Science, 10(5):1-7. https://doi.org/10.1007/s13201-020-01188-1

CHEN L. TIAN X., XIA D., NIE Y., LU L., YANG C., ZHOU Z. (2019) Novel colorimetric method for simultaneous detection and identification of multimetal ions in water: Sensitivity, selectivity, and recognition mechanism. ACS Omega 4(3), 5915-5922.

DUVAL B.D., CADOL D., MARTIN J., FREY B., TIMMONS S. (2020) Effects of the Gold King Mine spill on metal cycling through river and riparian biota. Ecosystem Services of Wetlands, 40:1033-1046. https://doi.org/10.1007/s13157-019-01258-4

FLOREA R.M., STOICA A.I., BAIULESCU G.E., CAPOTĂ P. (2005) Water pollution in gold mining industry: a case study in Roşia Montană district, Romania. Environmental Geology, 48(8):1132-1136. https://doi.org/10.1007/s00254-005-0054-7

HALL G., BUCHAR A., BONHAM-CARTER G. (2013) Quality control assessment of portable XRF analysers: Development of standard operation procedures, performance on variable media and recommended uses. Available online

at: https://www.appliedgeochemists.org/images/stories/XRF/pXRF%20Report%20Phase%20I%20Report%20rev%20Oct%202013.pdf (verified 28 Nov. 2020).

ISAAC R.A., KERBER J.D. (1971) Atomic absorption and flame photometry: Techniques and uses in soil, plant and water analysis. In: Walsh, L.M. (ed.). Instrumental methods for analysis of soils and plant tissue. American Society of Agronomy, Madison, WI.

KAGILIERY J., CHAKRABORTY S., ACREE A., WEINDORF D.C., BREVIK E.C., JELINSKI N.A., LI B., JORDAN C. (2019) Rapid quantification of lignite sulfur content: Combining optical and X-ray approaches. International Journal of Coal Geology, 216:103336. https://doi.org/10.1016/j.coal.2019.103336

KALNICKY D.J., SINGHVI R. (2001) Field portable XRF analysis of environmental samples. Journal of Hazardous Materials, 83(1-2):93-122. https://doi.org/10.1016/S0304-3894(00)00330-7

KINUTHIA G.K., NGURE V., BETI D., LUGALIA R., WANGILA A., KAMAU L. (2020) Levels of heavy metals in wastewater and soil samples from open drainage channels in Nairobi, Kenya: community health implication. Scientific Reports 10:8434. https://doi.org/10.1038/s41598-020-65359-5

KOCH J., CHAKRABORTY S., LI B., MOORE-KUCERA J., VAN DEVENTER P., DANIELL A., FAUL C., MAN T., PEARSON D., DUDA B., WEINDORF C.A., WEINDORF D.C. (2017) Proximal sensor analysis of mine tailings in South Africa: An exploratory study. Journal of Geochemical Exploration, 181:45-57. https://doi.org/10.1016/j.gexplo.2017.06.020

MASTEN S.J., DAVIES S.H., McELMURRY S.P. (2016) Flint water crisis: What happened and why? Journal of the American Water Works Association, 108(12):22-34. https://doi.org/10.5942/jawwa.2016.108.0195

McGLADDERY C., WEINDORF D.C., CHAKRABORTY S., LI B., PAULETTE L., PODAR D., PEARSON D., KUSI N.Y.O., DUDA B. (2018) Elemental assessment of vegetation via portable X-ray fluorescence (PXRF) spectrometry. Journal of Environmental Management, 210:210-225. https://doi.org/10.1016/j.jenvman.2018.01.003

NATIONAL RESOURCE DEFENSE COUNCIL (2018) Flint water crisis: Everything you need to know. Available online at https://www.nrdc.org/stories/flint-water-crisis-everything-you-need-know (verified 28 Nov. 2020).

PEARSON D., WEINDORF D.C., CHAKRABORTY S., LI B., KOCH J., DEVENTER P.V., WET J.D., KUSI N.Y. (2018) Analysis of metal-laden water via portable X-ray fluorescence spectrometry. Journal of Hydrology. https://doi.org/10.1016/j.jhydrol.2018.04.014

PEARSON D., CHAKRABORTY S., DUDA B., LI B., WEINDORF D.C., DEB S., BREVIK E., RAY D.P. (2017) Water analysis via portable X-ray fluorescence spectrometry. Journal of Hydrology. https://doi.org/10.1016/j.jhydrol.2016.11.018

PINTO M., DE R., ALMEIDA A.A. (2018) Trace elements in human milk. IntechOpen. Doi: 10.5772/intechopen.76436. R CORE TEAM (2020) R: A language and environment for statistical computing. R Foundation for Statistical Computing, Vienna, Austria. Available online at: http://www.Rproject.org (Verified on 29 March 2020).

RINCHEVAL M., COHEN D.R., HEMMINGS F.A. (2019) Biogeochemical mapping of metal contamination from mine tailings using field-portable XRF. Science of the Total Environment, 662:403-413. https://doi.org/10.1016/j.scitotenv.2019.01.235

ROUSSEAU R.M. (2009) The quest for a fundamental algorithm in X-ray fluorescence analysis and calibration. The Open Spectroscopy Journal, 3:31-42. https://doi.org/10.2174/1874383800903010031

SZYMCZYCHA-MADEJA A., WELNA M. (2013) Evaluation of a simple and fast method for the multi-elemental analysis in commercial fruit juice samples using atomic emission spectrometry. Food Chemistry, 141:3466-3472. https://doi.org/10.1016/j.foodchem.2013.06.067

SILVA S.H.G., RIBEIRO B.T., GUERRA M.B.B., DE CARVALHO H.W.P., LOPES G., CARVALHO G.S., GUILHERME L.R.G., RESENDE M., MANCINI M., CURI N., RAFAEL R.B.A., CARDELLI V., COCCO S., CORTI G., CHAKRABORTY S., LI B., WEINDORF D.C. (2021). PXRF in tropical soils: Methodology, applications, achievements and challenges. Advances in Agronomy, 167 https://doi.org/10.1016/bs.agron.2020.12.001

SHUTIC S., CHAKRABORTY S., LI B., WEINDORF D.C., SPERRY K., CASADONTE D. (2017) Forensic identification of pharmaceuticals via portable X-ray fluorescence and diffuse reflectance spectroscopy. Forensic Science International, 279:22-32. https://doi.org/10.1016/j.forsciint.2017.08.008

STEINER A.E., CONREY RM., WOLFF J.A. (2017) PXRF calibrations for volcanic rocks and the application of in-field analysis to the geosciences. Chemical Geology, 453:35-54. https://doi.org/10.1016/j.chemgeo.2017.01.023

THOMPSON V. (2007) Basic fundamental parameters in X-ray fluorescence. Spectroscopy, 22(5):46-50.

UDA M., ISHIZAKI A., SATOH R., OKADA K., NAKAJIMA Y., YAMASHITA D., OHASHI K., SAKURABA Y., SHIMONO A., KOJIMA D. (2005) Portable X-ray diffractometer equipped with XRF for archaeometry. Nuclear Instruments and Methods in Physics Research B 239:77-84. https://doi.org/10.1016/j.nimb.2005.06.214

VAN SPRANG H.A. (2000) Fundamental parameter methods in XRF spectroscopy. Advances in X-ray Analysis, 42:1-11.

UNITED STATES ENVIRONMENTAL PROTECTION AGENCY (2020ª) What is Superfund? Available online at: https://www.epa.gov/superfund/what-superfund (verified 6 Dec. 2020).

UNITED STATES ENVIRONMENTAL PROTECTION AGENCY (2020b) Emergency response to August 2015 release from Gold King Mine. Available online at: https://www.epa.gov/goldkingmine (verified 7 Dec. 2020).

UNITED STATES ENVIRONMENTAL PROTECTION AGENCY (2020c) Flint drinking water response. Available online at: https://www.epa.gov/flint (verified 7 Dec. 2020).

UNITED STATES GEOLOGICAL SURVEY (1993) Methods of analysis by the U.S. Geological Survey National Water Quality Laboratory – Determination of metals in water by inductively coupled plasma mass spectrometry. Available online at: https://pubs.usgs.gov/of/1992/0634/report.pdf (verified 6 Dec. 2020).

WEINDORF D.C., PEARSON D., CHAKRABORTY S. (2018) Portable apparatus for liquid chemical characterization. US Patent US10697953B2. Available online at: https://patents.google.com/patent/US10697953B2/en?oq=US10697953B2 (verified 6 Dec. 2020).

WEINDORF D.C., BAKR N., ZHU Y. (2014) Advances in portable X-ray fluorescence (PXRF) for environmental, pedological, and agronomic applications. Advances in Agronomy 128:1-45. http://dx.doi.org/10.1016/B978-0-12-802139-2.00001-9

WORLD HEALTH ORGANIZATION (2019) Sanitation. Available online at: https://www.who.int/en/news-room/fact-sheets/detail/sanitation (verified 28 Nov. 2020).

WORLD HEALTH ORGANIZATION (2020) Monitoring water sanitation and hygiene. Available online at https://www.who.int/activities/monitoring-water-sanitation-and-hygiene (verified 28 Nov. 2020).

ZIMMERMA, A.J., GUITIERREZ D.G., CAMPOS V.M., WEINDORF D.C., DEB S.K., CHACON S.U., LANDROT G., SIEBECKER M.G. (2021) Arsenic geochemistry in titanium dioxide (TiO_2) drinking water filter waste and impacted soils: Implications for urban environmental and human health. Env. Res. (Under Review).

ZHOU S., WEINDORF D.C., CHENG Q., YANG B., YUAN Z., CHAKRABORTY S. (2020a) Elemental assessment of vegetation via portable X-ray fluorescence: Sample preparation and methodological considerations. Spectrochimica Acta Part B: Atomic Spectroscopy, 174:105999. https://doi.org/10.1016/j.sab.2020.105999

ZHOU S., CHENG Q., WEINDORF D.C., YUAN Z., YANG B., SUN Q., ZHANG Z., YANG J., ZHAO M. (2020b) Elemental assessment of dried and ground samples of leeches via portable X-ray fluorescence. Journal of Analytical Atomic Spectrometry, 11:1:33. https://doi.org/10.1039/d0ja00328j

ZHOU, S., YUAN, Z., CHENG, Q., ZHANG, Z., YANG, J., 2018. Rapid in situ determination of heavy metal concentrations in polluted water via portable XRF: Using Cu and Pb as example. Environmental Pollution, 243(B):1325-1333. https://doi.org/10.1016/j.envpol.2018.09.087